AICS TECHNICAL REPORT
N0. 2017-001

Modification of a baroclinic test case to a height-based coordinate system without topography implementation

By

Ryuji Yoshida[1,2,] Hisashi Yashiro[1], Masaki Satoh[3], and Hirofumi Tomita[1,4]

1: RIKEN Advanced Institute for Computational Science,

7-1-26 Minatojima-minami-machi, Chuo-ku, Kobe, Hyogo 650—0047, Japan

2: Research Center for Urban Safety and Security, Kobe University, Kobe, Japan,

3: The University of Tokyo, Atmosphere and Ocean Research Institute, Kashiwa, Japan,

4: Japan Agency for Marine-Earth Science and Technology, Yokohama, Japan.

Modification of a baroclinic test case to a height-based coordinate system without topography implementation

Ryuji Yoshida[1,2], Hisashi Yashiro[1], Masaki Satoh[3], and Hirofumi Tomita[1,4]

1: RIKEN, Advanced Institute for Computational Science, Kobe, Japan,
2: Research Center for Urban Safety and Security, Kobe University, Kobe, Japan,
3: The University of Tokyo, Atmosphere and Ocean Research Institute, Kashiwa, Japan,
4: Japan Agency for Marine-Earth Science and Technology, Yokohama, Japan.

Abstract

In this study, a baroclinic wave test case is modified to be conducted without topography implementation in a model with a height-based vertical coordinate system (VCS). In the original test case, the topography implementation is required for a model with a height-based VCS, unlike a model with a pressure-based VCS. We propose a method to conduct the test case without the topography implementation using a model with a height-based VCS. Compared with the original test case, the proposed method provides similar wave structures and evolutions. The values and time evolutions of root mean square errors are almost the same as the original test case. The convergence of the numerical solution can be examined by the proposed method at a degree similar to that of the original method. This means that the proposed method examines the physical performance of the model without the topography implementation with a height-based VCS.

Corresponding author: Ryuji Yoshida, RIKEN Advanced Institute for Computational Science, 7-1-26 Minatojima-minami-machi, Chuo-ku, Kobe, Hyogo 650-0047, JAPAN.
E-mail: ryoshida@riken.jp
Tel: +81-78-940-5735
Fax: +81-78-304-4963

1 Introduction

Ideal test cases performed on the dynamical core of an atmospheric model are necessary to evaluate its physical performance and detect coding bugs. A test suite on the shallow water equation (Williamson et al. 1992) has been typically used as the standard test case to examine the physical performance of the two-dimensional dynamical core. As for a three-dimensional test case, Held and Suarez (1994) proposed a popular test case to investigate the physical performance climatologically. A deterministic test can directly detect the model error and/or the convergence of the numerical solution by calculating L2 norm, which represents the root mean square using the experimental results with a high-resolution result as the reference. Among the three-dimensional test cases, the baroclinic wave test cases are particularly useful as deterministic test cases, because the baroclinic wave is one of the most important phenomena for numerical weather prediction. Polvani et al. (2004) proposed a deterministic baroclinic wave test case for the three-dimensional global atmospheric model and realistic baroclinic waves were simulated in the test case. This type of test case is very useful because different amplitudes and phases of multiple waves can be examined by starting from a single perturbation rather than a periodic perturbation. However, the test case is not suitable to investigate the reproducibility of fine structures that appear in the high-resolution run, because this setting prescribes an explicit horizontal diffusion. Jablonowski and Williamson (2006a) developed a new baroclinic wave test case (hereafter JW06) that does not need the use of such a diffusion in their experimental setting. This provides a significant advantage to the evaluation of the convergence of the numerical solution. For this reason, JW06 has been recently used in model development as the standard test case for baroclinic waves (Skamarock et al. 2012, Ullrich and Jablonowski 2012, Park et al. 2014, Zangl et al. 2015).

The JW06 test case is applicable to a wide variety of models. However, the implementation of topography is also required when we conduct the JW06 test case on a height-based vertical coordinate system (VCS). The initial condition of the baroclinic state is defined by the hydrostatic balance on the pressure-based VCS. The geopotential field at the geoid surface with a meridional gradient must be given as the lower boundary condition. For height-based VCSs, the method of conversion of the initial pressure-based VCS to the height-based VCS is explained in JW06 to satisfy the lower boundary condition. As a result, the lower boundary condition of the geopotential field must be treated as "topography."

The topography implementation is one of the important steps of model design. It strongly affects the physical performance of the model. The physical performance of pure dynamical core should

be examined before applying the topography. Although the JW06 test case has been conducted in many models and will be used for many new models in the future, it has an above lack for the default use for height-based VCSs. Therefore, the JW06 test case should be applied to the height-based VCSs without topography implementation. Ullrich et al. (2014) has resolved this issue by a new analytical solution of initial condition. However, JW06 is still useful to compare results of a newly developed model with those of many models that have already conducted, because many knowledges in JW06 have been accumulated during long time so far.

In this study, we propose a modified method of the JW06 test case that enables to the dynamical core to function without topography implementation on the height-based VCS. The Non-hydrostatic ICosahedral Atmospheric Model (NICAM; Tomita and Satoh 2004; Satoh et al. 2008; 2014) was used to show the effectiveness of the modified method. We described the details of the modified JW06 test case method in Section 2 and discussed the experimental results of the modified method in comparison with the original test case in Section 3. Finally, we summarized the results in Section 4.

2   A modified method for the JW06 baroclinic wave test case

To describe the initial conditions, we assume five prognostic variables: three-dimensional wind speed components (*u, v, and w;* zonal, meridional and vertical velocities, respectively), potential temperature (*T*), and geopotential (*Φ*). In addition, a spherical coordinate with the pressure-based VCS is assumed. Temperature is indicated by $T(\lambda, \varphi, \eta)$, where λ is the longitude, φ is the latitude, and η is the vertical coordinate defined by a pressure-based hybrid coordinate system (Jablonowski and Williamson 2006b, defined as $\eta = A(\eta)p_0 + B(\eta)p_s$, where A and B are the specified coefficients. The coefficients are such that A = 0 and B = 1 at the bottom boundary (see Jablonowski and Williamson (2006b) for a detailed description of the setting of coefficients). p_0 and p_s denote the reference pressure (10^5 Pa) and surface pressure ($p_s = p_0 = 10^5$ Pa), respectively.

The initial conditions for the wind and potential temperature fields are defined based on JW06. In the JW06 test case, the auxiliary variable η_v is defined by

$$\eta_v = (\eta - \eta_0)\frac{\pi}{2} \tag{1}$$

with $\eta_0 = 0.252$. Using Eq. (1), the zonal wind speed is defined as

$$u(\lambda, \varphi, \eta) = u_0 \cos^{3/2}\eta_v \sin^2(2\varphi) \tag{2}$$

where $u_0 = 35$ ms^{-1} is the base wind speed. The structure of the zonal wind is zonally

homogenous. At the initial conditions, meridional and vertical wind speed components are set to zero,

$$v(\lambda, \varphi, \eta) = 0 \tag{3}$$

$$w(\lambda, \varphi, \eta) = 0 \tag{4}$$

The temperature field satisfying the thermal-wind balance with a given zonal wind is given by

$$T(\lambda, \varphi, \eta) = \langle T(\eta) \rangle + \frac{3}{4} \frac{\eta \pi u_0}{R_d} \sin \eta_v \cos^{1/2} \eta_v \times \left[\left\{ -2 \sin^6 \varphi \left(\cos^2 \varphi + \frac{1}{3} \right) + \right. \right.$$
$$\left. \left. \frac{10}{63} \right\} 2 u_0 \cos^{3/2} \eta_v + \left\{ \frac{8}{5} \cos^3 \varphi \left(\sin^2 \varphi + \frac{2}{3} \right) - \frac{\pi}{4} \right\} a \Omega \right] \tag{5}$$

where $a = 6.371229 \times 10^6$ m is the mean radius of the Earth and $\Omega = 7.29212 \times 10^{-5}$ s^{-1} is the angular velocity of the Earth. In Eq. (5), $\langle T(\eta) \rangle$ means horizontally averaged temperature and is defined by two different equations for different heights,

$$\langle T(\eta) \rangle = T_0 \eta^{R_d \Gamma / g}, \qquad \text{for } \eta_s \geq \eta \geq \eta_t \tag{6}$$

$$\langle T(\eta) \rangle = T_0 \eta^{R_d \Gamma / g} + \Delta T (\eta_t - \eta)^5, \quad \text{for } \eta_t > \eta \tag{7}$$

where $T_0 = 288$ K is the horizontally averaged temperature at the surface (p_s). Height level is specified by a dimensionless number and the surface level and tropopause level are $\eta_s = 1$ and $\eta_t = 0.2$, respectively. $\Delta T [K] = 4.8 \times 10^5$ is the empirical temperature difference. The dry ideal gas constant is $R_d = 287.0$ J kg^{-1}K^{-1} and the gravity acceleration is $g = 9.80616$ ms^{-1}. The geopotential field of the initial condition is defined by

$$\Phi(\lambda, \varphi, \eta) = \langle \Phi(\eta) \rangle + u_0 \cos^{3/2} \eta_v \times \left[\left\{ -2 \sin^6 \varphi \left(\cos^2 \varphi + \frac{1}{3} \right) + \right. \right.$$
$$\left. \left. \frac{10}{63} \right\} u_0 \cos^{3/2} \eta_v + \left\{ \frac{8}{5} \cos^3 \varphi \left(\sin^2 \varphi + \frac{2}{3} \right) - \frac{\pi}{4} \right\} a \Omega \right] \tag{8}$$

where

$$\langle \Phi(\eta) \rangle = \frac{T_0 g}{\Gamma} \left(1 - \eta^{R_d \Gamma / g} \right), \qquad \text{for } \eta_s \geq \eta \geq \eta_t \tag{9}$$

$$\langle \Phi(\eta) \rangle = \frac{T_0 g}{\Gamma} \left(1 - \eta^{\frac{R_d \Gamma}{g}} \right)$$
$$- R_d \Delta T \left\{ \left(\ln \left(\frac{n}{n_t} \right) + \frac{137}{60} \right) \eta_t^5 - 5 \eta_t^4 \eta + 5 \eta_t^3 \eta^2 - \frac{10}{3} \eta_t^2 \eta^3 + \frac{5}{4} \eta_t \eta^4 - \frac{1}{5} \eta^5 \right\}, \text{ for } \eta_t > \eta \tag{10}$$

Geopotential is used to solve the relationship between η-levels and height-levels with an iterative method based on Newton's method. The height-levels (z) are the prescribed values by a user. Based on JW06, the method is given by

$$\eta^{n+1} = \eta^n - \frac{F(\lambda, \varphi, \eta^n)}{(\partial F / \partial \eta)(\lambda, \varphi, \eta^n)} \tag{11}$$

where n denotes the iteration count and F is the forcing function given by

$$F(\lambda, \varphi, \eta^n) = -gz + \Phi(\lambda, \varphi, \eta^n) \tag{12}$$

$$\frac{\partial F}{\partial \eta}(\lambda, \varphi, \eta^n) = -\frac{R_d}{\eta^n} T(\lambda, \varphi, \eta^n) \tag{13}$$

The initial value of $\eta^0 = 10^{-7}$ is recommended in JW06 for the iterative method. The first estimated values are calculated using Eqs. (1), (2), and (5)-(10) with the value of η^0 and the estimated η^1 is updated using Eqs. (11)-(13). The absolute error $|\eta^{n+1} - \eta^n|$ decreases as iteration proceeds. When the absolute error decreases to a small enough value, the iteration is terminated. The final estimated values of the prescribed height-levels are used as the computationally analyzed initial state.

The definitions of the initial condition by Eqs. (2)-(10) are the same as the original JW06. The bottom boundary condition of the geopotential distribution at η_s is treated as the topography distribution for the height-based VCS in the original JW06 test case. This method requires an additional implementation of the topography scheme. In this study, we propose a modified method by converting from a geopotential distribution to a surface pressure distribution instead of the extra implementation of topography scheme. Referring to Jablonowski et al. (2008), the equation for the topography height (H) is given by substituting $\eta = \eta_s = 1$ in Eq. (8) and dividing it by gravitational acceleration g,

$$H\,[\text{m}] = \frac{u_0}{g} \cos^{\frac{3}{2}}\left((1 - \eta_0)\frac{\pi}{2}\right) \times \left[u_0 \cos^{\frac{3}{2}}\left((1 - \eta_0)\frac{\pi}{2}\right)\left\{\frac{10}{63} - 2\sin^6\varphi\left(\cos^2\varphi + \frac{1}{3}\right)\right\} + \right.$$
$$\left. a\Omega\left\{\frac{8}{5}\cos^3\varphi\left(\sin^2\varphi + \frac{2}{3}\right) - \frac{\pi}{4}\right\}\right]. \tag{14}$$

Using this topography height, we estimate the surface pressure. Pressure P_2 can be calculated using the reference pressure P_1 at a different height at the same horizontal location in the equation of hydrostatic balance,

$$P_2 = P_1 - \int_{z_1}^{z_2} \rho g dz \tag{15}$$

We estimate the surface pressure by extending Eq. (15) to the ground level and using the reference values for P_1 and z_1. We assume that the horizontal distribution of density is smooth and the density value is almost the same as the value at the neighboring location in the layer between z_1 and z_2. By this assumption, the surface pressure at the target location can be estimated by the height difference between the target location and the other location horizontally removed from the target. Thus, in Eq. (15), density (ρ) and height (z) are replaced by surface density (ρ_s) and topography height (H), respectively. Then, we obtain a relationship between the surface pressures of horizontally neighboring locations,

$$P_{S2} = P_{S1} - \int_{H_1}^{H_2} \rho_s g dH \tag{16}$$

where the suffixes (1, 2) for S and H indicate different latitudinal locations. ρ_s can be obtained by the state equation of an ideal gas using the predetermined surface temperature and topography height from Eqs. (5) and (14). To calculate P_{S2}, P_{S1} should be a known reference value. The surface pressure at η_s is $p_s = 10^5$ Pa and topography (i.e., geopotential height at η_s) is 0 m at latitude φ_{ref}, derived from Eq. (14) by assigning 0 m to H and solving for φ ($\varphi_{ref} =$ 0.691590985442682 rad). We call P_{S1}, at this latitude, the reference surface pressure $P_{S(\varphi_{ref})}(= 10^5$ Pa), and H, at this latitude, the reference topography height $H_{(\varphi_{ref})}(= 0$ m). We can then calculate the surface pressure everywhere using $P_{S(\varphi_{ref})}$ and $H_{(\varphi_{ref})}$.

To apply the modified method to the atmospheric models, we discretized the integration in Eq. (16) through the trapezoidal rule,

$$P_{S(\varphi_{(j)})} = P_{S(\varphi_{ref})} - g\left(\frac{\rho_{s(\varphi_{ref})}+\rho_{s(\varphi_{(j)})}}{2}\right)\left(H_{(\varphi_{(j)})} - H_{(\varphi_{ref})}\right) \qquad (17)$$

where j is the meridional grid point index. We used the same reference point (φ_{ref}) for all latitudinal locations so as to easily calculate the grid points according to the tested model. Although $P_{S(\varphi_{(j)})}$ can be calculated by replacing φ_{ref} in the neighboring grid point of j iteratively, the result is not different from the case using a constant φ_{ref}. Furthermore, using the relationship $\rho_s = \frac{P_s}{R_d T_s}$, Eq. (17) is transformed as

$$P_{S(\varphi_{(j)})} = \frac{P_{s(\varphi_{ref})}\left(1-g\left(H_{(\varphi_{(j)})}-H_{(\varphi_{ref})}\right)/2R_d T_{s(\varphi_{ref})}\right)}{1+g\left(H_{(\varphi_{(j)})}-H_{(\varphi_{ref})}\right)/2R_d T_{s(\varphi_{(j)})}},$$

where $T_{s(\varphi)}$ is the surface temperature, derived from Eq. (5) by assigning η_s to η. The distribution of surface pressure is determined by repeating this calculation for all grid points in the meridional direction. The vertical pressure profile is calculated using the equation of hydrostatic balance (Eq. [15]) by vertical integration with the surface pressure as a lower boundary condition for the prescribed height-levels. Up to this point, the steady state of initial conditions is given for the height-based VCS without topography. The results of the steady state test case are explained in Section 3.

For the wave developing experiment, an initial perturbation is required. Following JW06, the initial perturbation is defined by

$$u'(\lambda, \varphi, \eta) = u_p \exp\{-(r/L)^2\},$$

where $L = a/10$ denotes the horizontal perturbation scale. r is defined by

$$r = a \arccos\{\sin \varphi_c \sin \varphi + \cos \varphi_c \cos \varphi \cos(\lambda - \lambda_c)\},$$

where $\lambda_c = \pi/9 , \varphi_c = 2\pi/9$ is the location of the initial perturbation and the perturbation is

6

located at 20°E/40°N. In addition, the friction at the lower boundary should be neglected, i.e., slip condition.

3 Test experiments of the modified method

3.1 Experimental settings

Recently, various global models with height coordinates have been developed, such as the Model for Prediction Across Scales (MPAS, Skamarock et al. 2012) and the ICOsahedral Non-hydrostatic (ICON) model (Zangl et al. 2015). In this study, we used NICAM (Tomita and Satoh 2004; Satoh et al. 2008; 2014) to examine the modified method of the JW06 test case. The horizontal discretization of NICAM is an icosahedral grid system with an Arakawa A-grid on the sphere and the vertical grid coordinate is a height-based VCS with a Lorenz type staggered grid. The topography representation is implemented by the terrain following coordinate. The temporal discretization is the third order Runge-Kutta scheme and an explicit numerical filter based on the fourth order hyper-diffusion is used. Although the native grid topology in NICAM is an icosahedral grid system, each of the grid points has the latitude-longitude information. Therefore, the initial state can be directly calculated by the method described in Section 2.

We used two different horizontal resolutions and three different vertical grid configurations to examine resolution dependency. The horizontal grid spacings were 240 km (glevel-5) and 120 km (glevel-6), where "glevel-n" represents the horizontal grid resolution in the icosahedral grid, generated by the nth recursive division (Tomita et al. 2001). The vertical grid arrangements had 40,
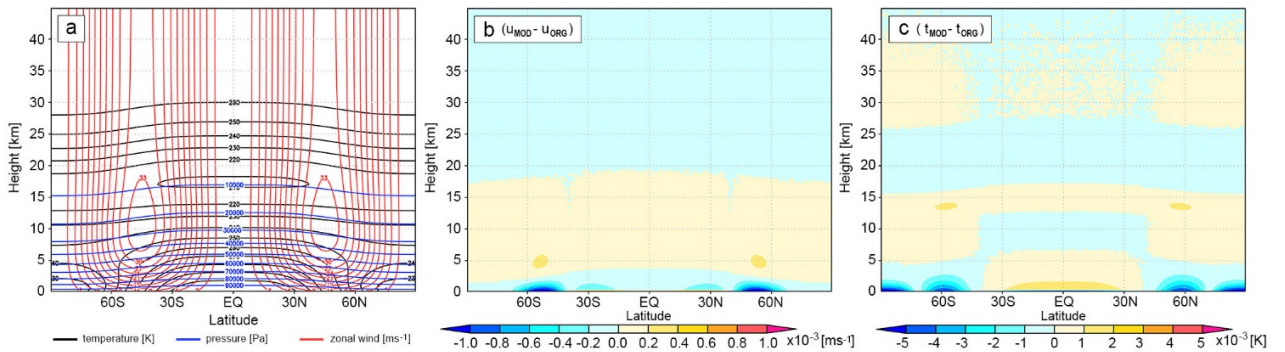

Fig. 1 The initial condition in glevel-6 (120 km) with 160 levels. (a) The initial condition calculated by the modified method. Black contours represent temperature, blue contours represent pressure, and red contours represent zonal wind speed. The structure is homogenous in the longitudinal direction. (b) and (c) are the difference of zonal wind speed ($u_{MOD} - u_{ORG}$) and the difference of temperature ($t_{MOD} - t_{ORG}$), respectively. ORG means the original method and MOD means the modified method.

Table 1 Experimental model settings

Settings	G-level 5	G-level 6
horizontal grid space (km)	240	120
vertical levels	40, 80, 160	40, 80, 160
model top height (km)	45	45
DT (sec)	600	300
numerical diffusion	4th order hyper-diffusion	4th order hyper-diffusion
diffusion coefficient ($m^4 s^{-1}$)	1.20×10^{16}	1.50×10^{15}

80, and 160 levels with a constant grid spacing of 1,125.0, 562.6, and 281.3 m, respectively. We conducted two types of experiments: a steady state experiment (without an initial perturbation) and a wave developing experiment. The time integration period was 30 d for the steady state experiment and 12 d for the wave developing experiment. Other experimental settings are shown in Table 1. The calculated initial condition in glevel-6 with 160 levels is shown in Fig. 1. The zonal wind jet, temperature, and pressure fields were symmetrically distributed with respect to the equator (Fig. 1a). The difference between the zonal wind speeds ($u_{diff} = u_{MOD} - u_{ORG}$) and the difference between the temperatures ($t_{diff} = t_{MOD} - t_{ORG}$) are shown in Fig. 1(b) and (c), respectively. The maximum wind speed difference was approximately $|1 \times 10^{-3}|$ ms^{-1} that is 0.003% of the base wind speed (35 ms^{-1}). The temperature difference was also small, approximately $|5 \times 10^{-3}|$ K that is 0.002% of the horizontally averaged surface temperature T_0 (288 K). Therefore, the initial condition of the modified method was almost the same as the original method.

3.2 Experimental results

To examine the impact of changing the initial condition using the modified method, we compared the results of the steady state experiment using the modified method (MOD) with those obtained using the original method (ORG). For the analysis, we used a latitude-longitude grid data converted from the original icosahedral grid system using linear interpolation. To evaluate the effect of maintaining the initial state, we calculated the root mean square error L2 norm by referring to JW06.

$$\text{L2 norm}\left(\overline{u850} - \overline{u850}_{t0}\right) = \left[\frac{\Sigma_j \{\overline{u850}(\varphi_j, t) - \overline{u850}(\varphi_j, t0)\}^2 \omega_j}{\Sigma_j \omega_j}\right]^{1/2},$$

where the over bar $\overline{(\ )}$ denotes the zonal average, t0 denotes the initial time, $\omega_j = |\sin \varphi_{j+1/2} - \sin \varphi_{j-1/2}|$ is the weighting function where the half indices denote the locations of
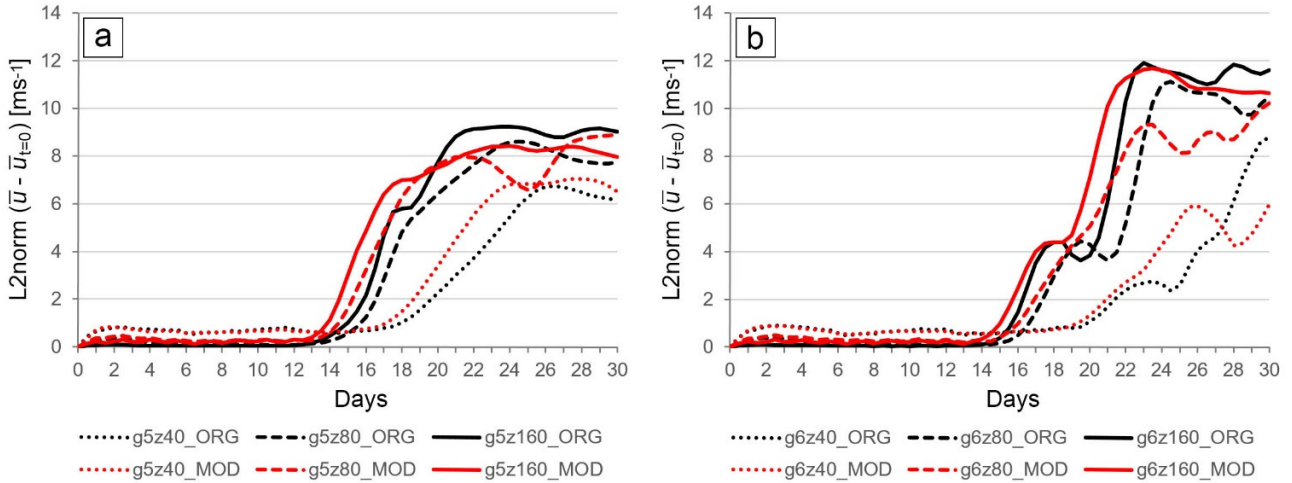
8

Fig. 2 L2 norm (root mean square error) of zonal wind speed at 850 hPa (U850) for the steady state experiment for (a) glevel-5 (g5; 240 km) and (b) glevel-6 (g6; 120 km). ORG means the original method and MOD means the modified method.
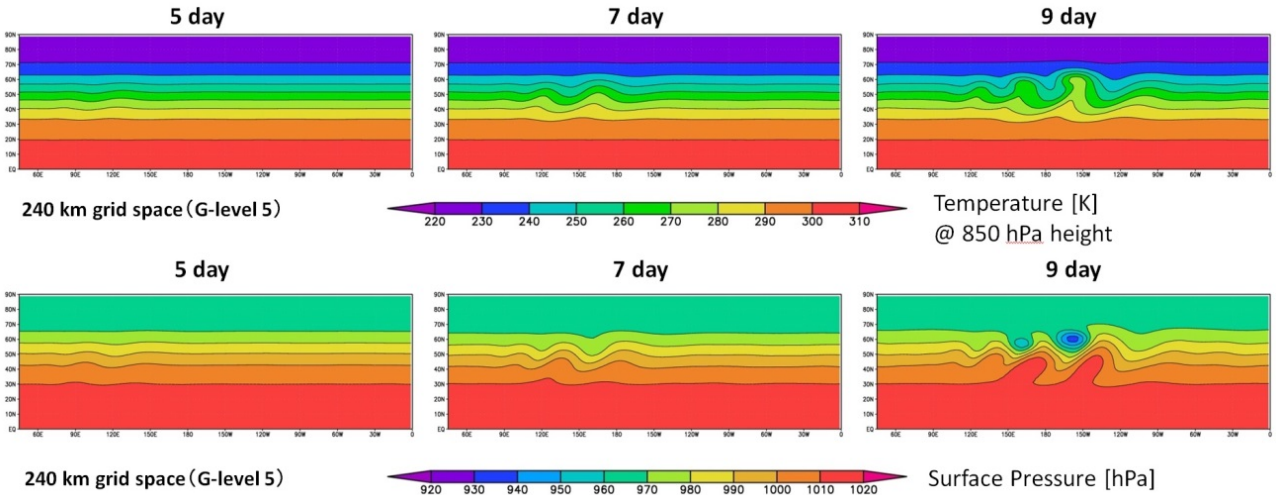

Fig. 3 Temperature and surface pressure distributions for the modified method in glevel-5 (240 km) with 160 vertical levels. Only the northern hemisphere is shown in each panel.

cell interfaces in the meridional direction. The temporal evolutions of L2 norm are shown in Fig. 2 for both glevel-5 and glevel-6. For all experimental settings, the initial state is maintained with an error less than 1 ms^{-1} for the first ten days. An error of 1 ms^{-1} is about 3% of the base wind speed (35 ms^{-1}). The period in which the initial state is maintained with less than 1 ms^{-1} of error is called "the quasi steady state (QSS) period" hereafter. The error rapidly increased around day 13 for glevel-5 and around day 15–16 for glevel-6. Because the accuracy of the horizontal partial difference in glevel-6 was higher than that in glevel-5, the QSS period in glevel-6 was longer than that in glevel-5. The length of the QSS period in MOD was similar to that in ORG for each horizontal grid space. Therefore, the initial condition of MOD satisfies a balance similar to ORG. The error was reduced at higher vertical resolutions during the QSS period. In glevel-6 of MOD,
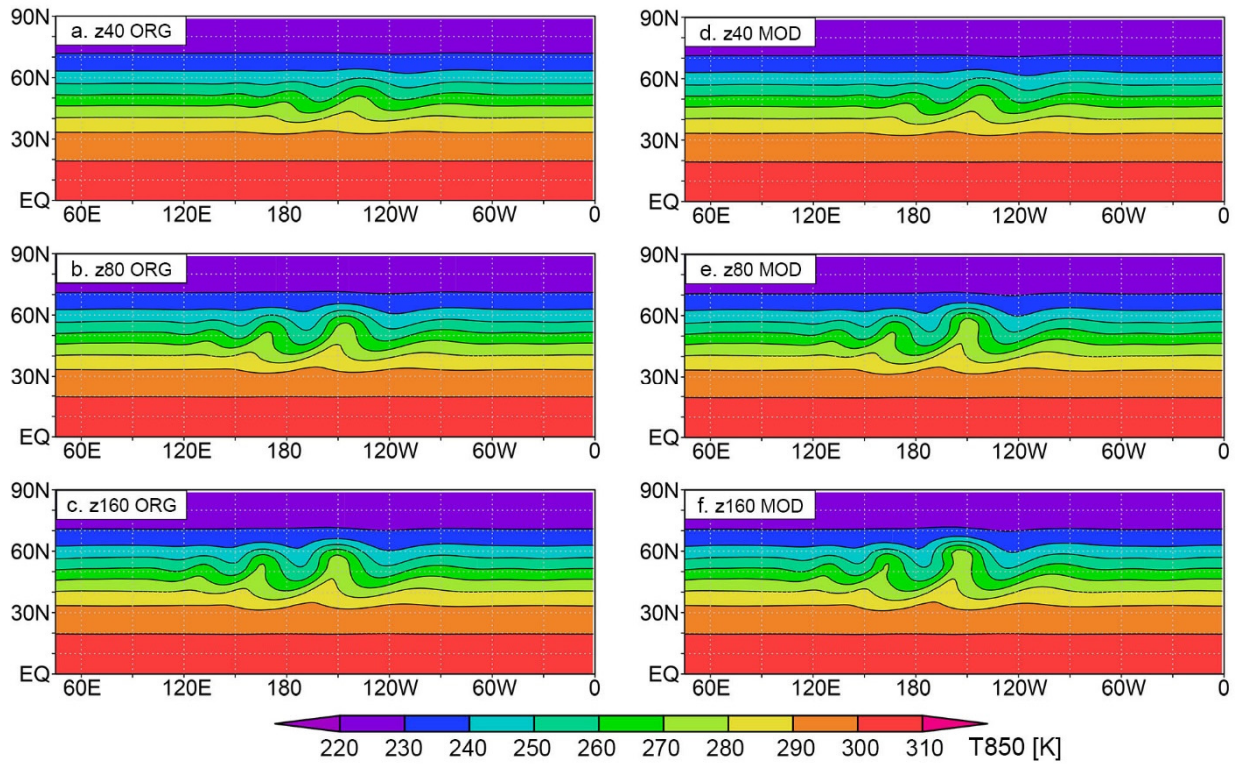
Fig. 4 Temperature distribution at 850 hPa on day 9 in glevel-5 (240 km). Only the northern hemisphere is shown in each panel. ORG means the original method and MOD means the modified method.
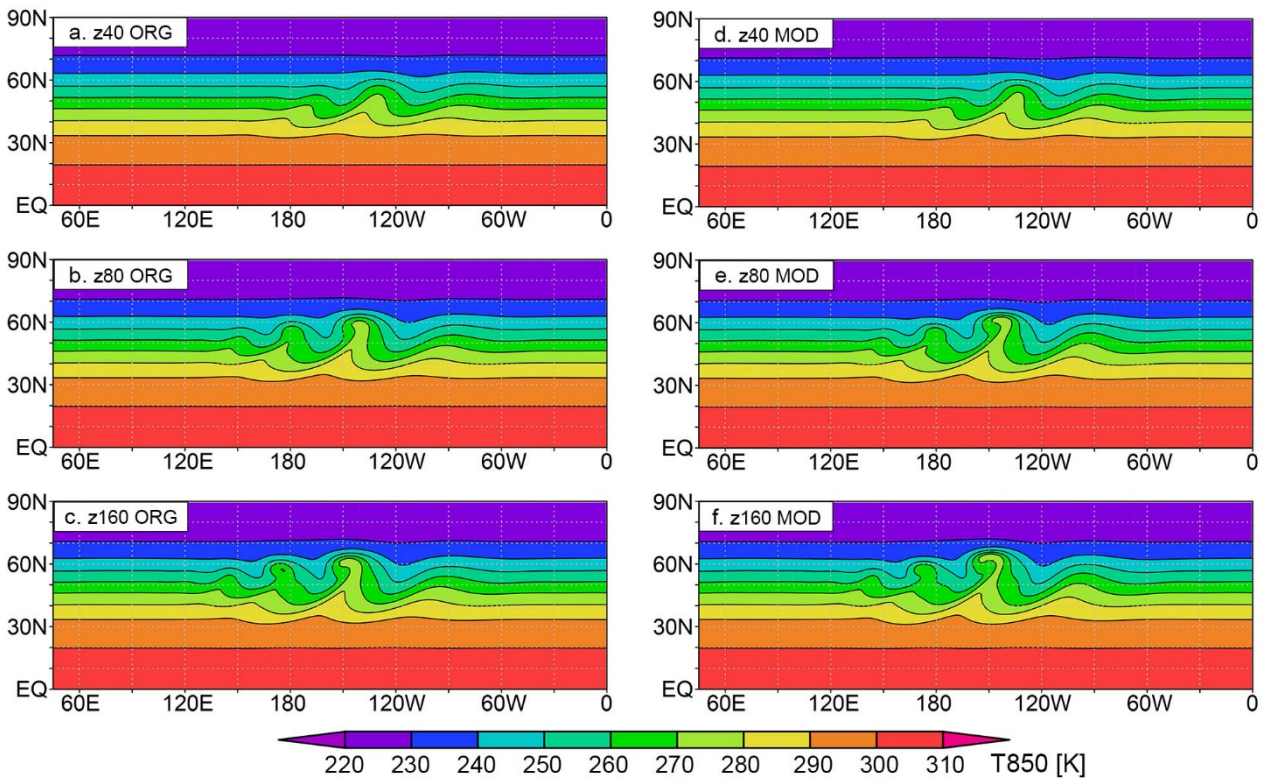
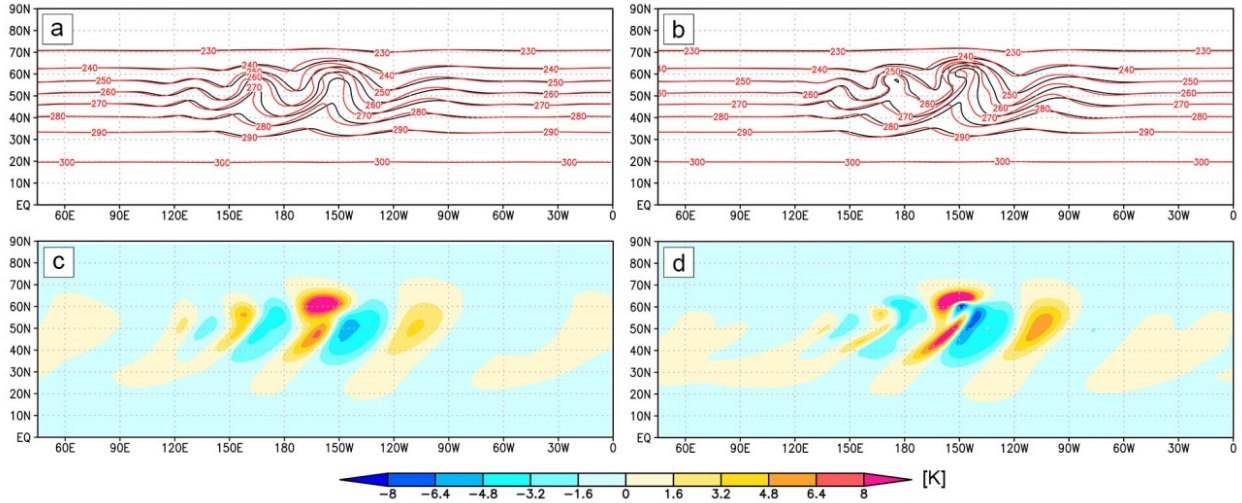

Fig. 5 Same as Fig. 4 but for glevel-6 (120 km).

Fig. 6 Temperature distributions at 850 hPa on day 9 for (a) and (b), and the difference of the temperature distribution ($t850_{MOD} - t850_{ORG}$) for (c) and (d). (a) and (c) are glevel-5 (240 km) with 160 vertical levels, and (b) and (d) are glevel-6 (120 km) with 160 vertical levels. The back contour is ORG and red contour is MOD. ORG means the original method and MOD means the modified method.

the average error values for 40, 80, and 160 levels were 0.7, 0.3, and 0.2 ms^{-1}, respectively. The QSS period tended to be shorter for higher vertical resolutions regardless of horizontal grid spaces and methods of initial state creation. Further investigation of these characteristics is needed in future studies.

We next explain the results of the wave developing experiment. Figure 3 shows the development of the simulated waves in MOD with glevel-5 and 160 vertical levels. It is clear from the surface pressure field that several mid-latitudinal lows have developed by day 9. Figures 4 and 5 show the temperature distributions for glevel-5 and glevel-6, respectively. The structure of the temperature distribution in MOD was quite similar to that in ORG (Figs. 4 and 5). To clarify these characteristics, the temperature distribution on day 9 of MOD was compared directly to that of ORG for glevel-5 and glevel-6 with 160 levels (Fig. 6). The horizontal structure of the temperature for MOD was similar to that of ORG regardless of horizontal grid spaces. Although the locations of the wave phases in MOD were slightly shifted westward compared with those in ORG (Fig. 4a and 4b), the structure of the simulated waves in MOD was qualitatively the same as that in ORG. Thus, the modified method in the height-based coordinate model has the potential to simulate the baroclinic waves as well as the original method in pressure-based coordinate models.

Comparison of different vertical resolutions (Fig. 4a with Fig. 4c, or Fig. 4d with Fig. 4f) showed that the wave structure sharpened with an increasing number of vertical levels and this is a common feature of ORG and MOD. Comparison of different horizontal grid spaces (Fig.4c with Fig. 5c or
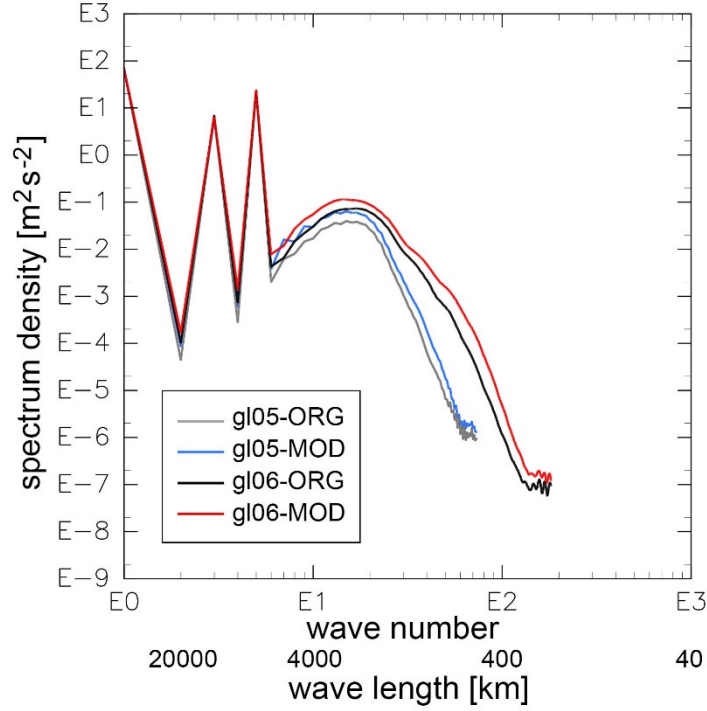
11

Fig. 7 Spectral density of zonal wind speed at 850 hPa for the wave developing experiment with 160 vertical levels. ORG means the original method and MOD means the modified method.

Fig. 4f with Fig. 5f) showed that the wave structure of glevel-6 was sharper than that of glevel-5, and this is the same in the other vertical grid settings. The power spectral density of zonal wind speed at 850 hPa is shown in Fig. 7 for both glevel-5 and glevel-6 with 160 vertical levels. The spectral density in glevel-5 was similar to that in glevel-6 around 3,000 km of wavelength (Fig. 7). Since this wavelength corresponds to that of the baroclinic wave, the outlines of the waves were simulated with a similar magnitude in both glevel-5 and glevel-6. The spectral density at wavelengths shorter than 3,000 km in glevel-6 was much higher than that in glevel-5. This indicates that the numerical solution is refined by increasing the horizontal resolution. These characteristics in MOD are the same as in ORG in terms of the correspondence between the original and modified test cases. Thus, the simulated phenomenon in MOD is the same as that in ORG. Although topography implementation is necessary in ORG, it is not required in MOD.

To assess the error in the wave developing experiment, we calculated the L2 norm of the zonal wind speed at 850 hPa. We assume that the results of the numerical simulation with high resolution are close to the real solution. Thus, L2 norm is defined as,

$$\text{L2 norm} = \left[\frac{\sum_i \sum_j \{u850(\lambda_i, \varphi_j, t) - u850_{\text{ref}}(\lambda_i, \varphi_j, t)\}^2 \omega_j}{\sum_i \sum_j \omega_j} \right]^{1/2} \tag{18}$$

where $u850$ and $u850_{\text{ref}}$ denote the data of the assessment target and of the reference solution,
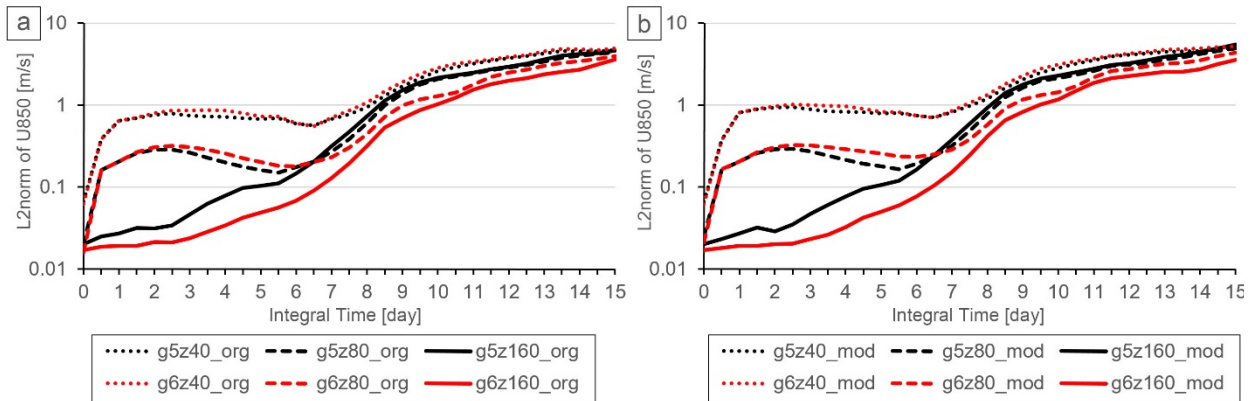
12

Fig. 8 L2 norm (root mean square error) of zonal wind speed at 850 hPa (U850) for the wave developing experiment using (a) the original method (ORG) and (b) the modified method (MOD).
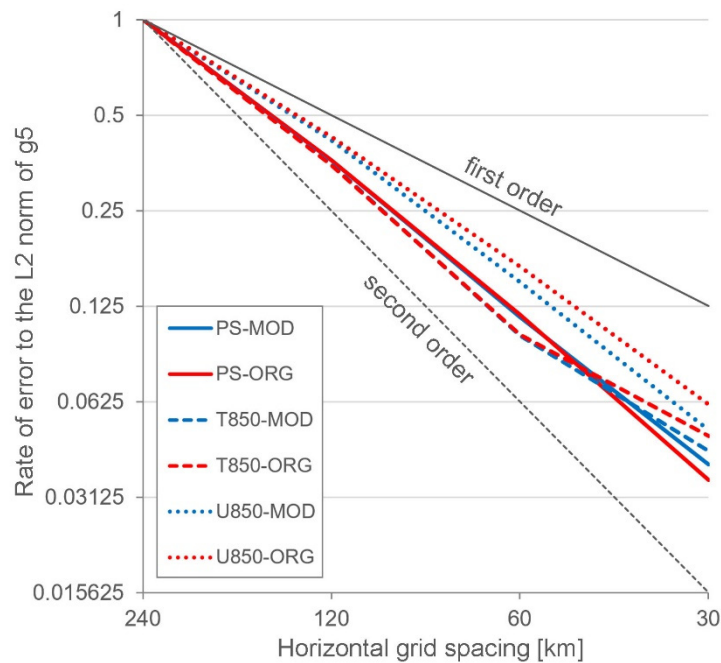

Fig. 9 Slope of the convergence for numerical solution. Rate of error (R) is calculated as $R = L2\,norm/L2norm_{g5}$, where $L2\,norm$ is root mean square error for surface pressure (PS), temperature at 850 hPa (T850), and zonal wind speed at 850 hPa (U850) for each horizontal grid spacing. $L2\,norm_{g5}$ is root mean square error of g-level 5 (240 km) for each variable. All of L2 norm are calculated on the 7th day after the initial time.

respectively. The simulated result by NICAM in 14-km horizontal grid spacing with 160 vertical levels was used as the reference solution. L2 norm for ORG and MOD are shown in Fig. 8 (a) and (b), where the reference solution is used with the same initial state method as each assessment target. The error rapidly increased with time in settings with 40 and 80 vertical levels regardless of the horizontal grid spacing because of an imbalance in the initial condition with respect to the non-hydrostatic model (Skamarock et al. 2012). The error decreased after day 3 and the initial

13

shock became steady by day 5 in glevel-5 cases. Note that this not only occurred in MOD but also in ORG. The initial shock can be reduced by recalculating the initial state of the wind field based on the thermal-wind balance (Skamarock et al. 2012). The initial error is much lower in the results of the cases with 160 vertical levels both for ORG and MOD. The wave patterns became significant on day 5 and one of the waves reached maturity by day 9 (Fig. 3). Comparing Fig. 8(b) with (a), the error of MOD was quite close to that of ORG and the temporal variation of MOD was similar to that of ORG. The error increased rapidly from day 4 to day 9 because the baroclinic waves developed rapidly during this period. This period was the focus point of the baroclinic wave test case. In this period, the error exceeded 1 ms^{-1} that was smaller than the error of the steady state test case with 80 or 160 vertical levels. Therefore, MOD has the potential to evaluate the model performance with the same degree of error as ORG and could be applied for comparing the model performance with pressure-based VCS.

Examining the convergence of the numerical solution is important for the deterministic test case. We examined the convergence using the L2 norm for both ORG and MOD on the 7th day after the initial time. For an accurate assessment, we performed additional calculations with finer horizontal grid spacings: 60 km (glevel-7), 30 km (glevel-8), and 14 km (g-level 9). The vertical grid configurations had 160 levels for each horizontal grid spacing and other settings were the same as the experiments above. To evaluate the convergence of the numerical solution, the results from the 14-km grid spacing were used as the reference solution in L2 norm calculation by Eq. (18). The convergence for four different horizontal grid spacings is shown in Fig. 9. The slope of NICAM was between the first order and the second order slopes regardless of the variables. Since the horizontal discretization of NICAM is a second-ordered scheme, the performance in Fig. 9 is reasonable. The measured performance of the convergence in MOD was almost the same as that in ORG. Therefore, we can examine the convergence by using MOD without terrain implementation on the model of the height-based VCS.

4   Summary

In this study, we propose a modified method of the baroclinic wave test case of JW06 for global atmospheric models. Topography implementation is not required to conduct the test case on a model with a height-based VCS. In the original method, the test case is not able to perform the dynamical core without the topography implementation. In the modified method, the topography profile is converted to surface pressure, keeping the consistency between the horizontal and

vertical balances. We examined the modified method using NICAM. In the steady state experiment, the period during which the initial state was maintained with an error of less than 1 ms^{-1} in u850 was similar in length for MOD and ORG. In the wave developing experiment, the error of the modified method in the wave developing period was quite similar to that of the original method. The simulated baroclinic waves in the modified method were close to those in the original method with respect to wave structures and phases. The modified method can examine the convergence of the numerical solution at degree similar to that of the original method, i.e., by using the modified method proposed in this study, the baroclinic wave test case of JW06 becomes a more useful test case for examining the model performance in the early stages of global atmospheric model development with the height-based VCS.

Acknowledgements

References

Held I. M., and M. J. Suarez, 1994: A proposal for the intercomparison of the dynamical cores of atmospheric general circulation models. *Bull. Am. Meteorol. Soc.*, **75**, 1825–1830.

Jablonowski C., and D. L. Williamson, 2006a: A baroclinic instability test case for atmospheric model dynamical cores., *Q. J. R. Meteorol. Soc.*, **132**, 2943–2975.

Jablonowski C., and D. L. Williamson, 2006b: A baroclinic wave test case for dynamical cores of general circulation models: Model intercomparisons. NCAR Technical Note NCAR/TN-469+STR, available online at http://www.library.ucar.edu/uhtbin/hyperion-image/DR000790 or http://www-personal.umich.edu/~cjablono/TN-469+STR.pdf

Jablonowski C., P. Lauritzen, R. Nair, and M. Taylor, 2008: Idealized test cases for the dynamical cores of Atmospheric General Circulation Models: A proposal for the NCAR ASP 2008 summer colloquium, available from http://www-personal.umich.edu/~cjablono/NCAR_ASP_2008_idealized_testcases_29May08.pdf

Park S., J. B. Klemp, and W. C. Skamarock, 2014: A Comparison of Mesh Refinement in the

Global MPAS-A and WRF Models Using an Idealized Normal-Mode Baroclinic Wave Simulation. *Mon. Wea. Rev.*, **142**, 3614–3634.

Polvani L. M., R. K. Scott, and S. J. Thomas, 2004: Numerically converged solutions of the global primitive equations for testing the dynamical core of atmospheric GCMs. *Mon. Wea. Rev.*, **132**, 2539–2552.

Satoh M., T. Matsuno, H. Tomita, H. Miura, T. Nasuno, and S. Iga, 2008: Nonhydrostatic icosahedral atmospheric model (NICAM) for global cloud resolving simulations. *J. Comput. Phys.*, **227**, 3486–3514.

Satoh M., H. Tomita, H. Yashiro, H. Miura, C. Kodama, T. Seiki, A. T. Noda, Y. Yamada, D. Goto, M. Sawada, T. Miyoshi, Y. Niwa, M. Hara, T. Ohno, S. Iga, T. Arakawa, T. Inoue, and H. Kubokawa,, 2014: The Non-hydrostatic Icosahedral Atmospheric Model: Description and Development. *Progress in Earth and Planetary Science*, **1**, 18. doi:10.1186/s40645-014-0018-1.

Skamarock W. C., J. B. Klemp, L. D. Fowler, M. G. Duda, S.-H. Park, and T. D. Ringler, 2012: A multiscale nonhydrostatic atmospheric model using centroidal Voronoi tesselations and C-grid staggering. *Mon. Wea. Rev.*, **140**, 3090–3105.

Tomita H., M. Tsugawa, M. Satoh, and K. Goto, 2001: Shallow water model on a modified icosahedral geodesic grid by using spring dynamics. *J. Comput. Phys.*, **174**, 579–613.

Tomita H., and M. Satoh, 2004: A new dynamical framework of nonhydrostatic global model using the icosahedral grid. *Fluid Dyn. Res.*, **34**, 357–400.

Ullrich P.A, and C. Jablonowski, 2012: MCore: A non-hydrostatic atmospheric dynamical core utilizing high-order finite-volume methods. *J. Comput. Phys.,* **231**, 5078–5108.

Ullrich P.A, T. Melvin, C. Jablonowski, and A. Staniforth, 2014: A proposed baroclinic wave test case for deep- and shallow-atmosphere dynamical cores. *Q. J. R. Meteorol. Soc.*, **140**, 1590–1602.

Zangl G., D. Reinert, P. Ripodas, and M. Baldauf, 2015: The ICON (icosahedral non-hydrostatic) modelling framework of DWD and MPI-M: Description of the non-hydrostatic dynamical core. *Q. J. R. Meteorol. Soc.*, 141, 563–579, doi: 10.1002/qj.2378.

Williamson, D. L., J. B. Drake, J. J. Hack, R. Jakob, and P. N. Swarztrauber, 1992: A standard test set for numerical approximations to the shallow water equations in spherical geometry. J. Comput. Phys., **102**, 211–224.